ACS OMEGA

http://pubs.acs.org/journal/acsodf

Article

Synthesis, Characterization, and CO_2 Uptake of Adsorbents Prepared by Hydrothermal Carbonization of Chitosan

José A. O. Chagas, Gustavo O. Crispim, Bianca P. Pinto, Rosane A. S. San Gil, and Claudio J. A. Mota*

Cite This: *ACS Omega* 2020, 5, 29520−29529

Read Online

ACCESS | Metrics & More | Article Recommendations | Supporting Information

ABSTRACT: Chitosan, a heteropolysaccharide obtained from the N-deacetylation of chitin, has stood out as a raw material to produce CO_2 adsorbents. In this work, we report the hydrothermal carbonization (HTC) of chitosan for different times and the potential of the materials for CO_2 adsorption. Elemental analysis indicated that the carbon weight content increases, whereas the relative amount of oxygen atoms decreases upon increasing the time of HTC. The relative nitrogen content was almost constant, indicating that HTC did not lead to significant loss of nitrogenated compounds. FTIR and ^{13}C MAS/NMR spectra suggest that the structure of the sorbents becomes more aromatic with the increase of HTC time. The thermal properties of HTC materials were similar to that of chitosan, whereas their basicity was less compared to that of the parent chitosan. SEM images did not show significant porosity, which was confirmed by the BET area of the materials, around 2 $m^2 \cdot g^{-1}$, similar to that of the parent chitosan. The materials were tested for CO_2 capture at 25 °C and 1 bar; the HTC chitosan adsorbents showed CO_2 uptakes about 4-fold higher than that of the parent chitosan. The adsorption process was better described by the Freundlich isotherm and the pseudo-second-order kinetic model.

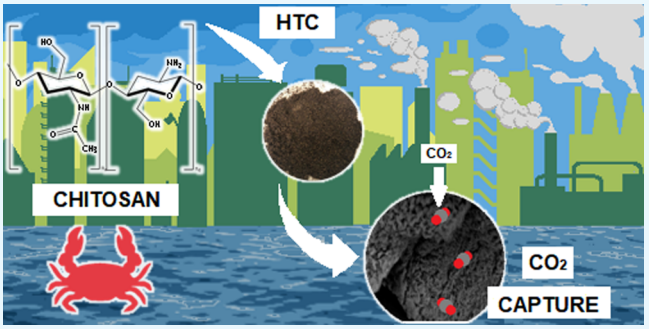

INTRODUCTION

The increasing growth of population and demand for energy at the beginning of the 21st century are jeopardizing the sustainability of the planet. Fossil fuels will still share a major proportion of the world's energy matrix in the forthcoming decades, impacting the environment and causing global warming through the increase of CO_2 concentration in the atmosphere.[1,2] Therefore, decreasing the carbon emissions is strategic to meet the goals set out in international climate protocols, such as the Paris Agreement.[3,4]

CO_2 capture has been considered as a potential technology to reduce the anthropic emissions of this gas, especially in postcombustion processes. Today, most of the available technologies pertain to absorption and stripping with aqueous basic solutions.[5,6] Nevertheless, there are some drawbacks associated with the use of solvents, especially the high-energy input to recover the captured CO_2.[7] On the other hand, the development of adsorbents for CO_2 capture is growing rapidly. Materials such as activated carbon,[8] mesoporous silica,[9] zeolite,[10] alumina,[11] and polymers[12] have been studied lately. Considering the acidic character of the CO_2 molecule, basic solid sorbents can be prepared through physical impregnation or chemical grafting of an amine compound onto the surface of a support.[13] However, the synthesis of these adsorbents has some disadvantages, such as the high cost and leaching of amine compounds, as well as their potential harmful properties.[14]

From an environmental standpoint, the use of biomass to prepare adsorbents for CO_2 capture emerges as a promising possibility. Notably, biomass use is regarded not only from an environmental point of view, preventing the use of fossil-derived compounds, but also from an economic perspective, as many biomass materials are cheap and abundant.[15] Biomass from residues, mainly associated with agricultural and forestry operations, represents a potential sustainable source for the development of adsorbents for CO_2 capture.[16]

Chitosan, a polysaccharide with an amino functionality, has been reported as a precursor to adsorbents for CO_2 capture.[14,17,18] It is obtained from the N-deacetylation of chitin, one of the most abundant natural polymers in the world, which may be extracted from the carapace and exoskeleton of crustaceans.[19] The presence of free amino groups in the structure of chitosan can provide basic sites for the adsorption of CO_2, similar to other amino-based adsorbents.[20] Indeed, it has been reported that chitosan-based sorbents can capture the CO_2 molecule through the

Received: September 11, 2020
Accepted: October 20, 2020
Published: November 3, 2020

https://dx.doi.org/10.1021/acsomega.0c04470
ACS Omega 2020, 5, 29520−29529

Table 1. CHN Elemental Analysis of Chitosan and HTC Samples

sample	C (wt %)	H (wt %)	N (wt %)	O (wt %)	HHV ($MJ \cdot kg^{-1}$)
CHIT	39.8	6.8	7.3	46.1	
CHIT-HTC-1	41.2	7.0	7.7	44.1	16.0
CHIT-HTC-2	40.8	7.0	7.6	44.7	15.8
CHIT-HTC-4	41.2	6.5	7.5	44.8	15.2
CHIT-HTC-6	41.5	7.0	7.6	44.0	16.2
CHIT-HTC-12	41.7	6.8	7.4	44.1	15.9
CHIT-HTC-24	43.7	6.8	7.3	42.2	16.9
CHIT-HTC-48	48.6	6.3	7.5	37.6	18.7

formation of ammonium carbamates, at room temperature, releasing the adsorbed gas upon heating.[21,22] However, pure chitosan has a low CO_2 adsorption capacity and most of the studies using chitosan-derived sorbents aim to maximize the CO_2 adsorption capacity through changes in the surface properties.[23−25]

The hydrothermal carbonization (HTC) of biomass is a thermochemical process that takes place under moderate heating conditions (120−250 °C) and autogenous pressure, in the presence of water, giving rise to water-soluble substances and a carbon-rich material.[26,27] This process is simple, with low production costs, and does not make use of organic solvents, catalysts, or surfactants. Therefore, the HTC has been pointed out as a green procedure, which allows the improvement of the adsorption properties of biomass-derived materials and the synthesis of functionalized carbons.[28−30]

Some HTC studies were performed to achieve changes in the textural and structural properties of chitosan while trying to keep the amine groups that may favor adsorption and other processes. For instance, Simsir et al. produced carbonaceous solids, with a dense surface and a carbon content between 47 and 64 wt %, through the HTC of chitosan at 200 °C between 6 and 48 h of treatment.[27] Texter et al. reported that a hydrochar of chitosan could be obtained upon HTC at 180 °C for 20 h, with 79.2 wt % of carbon content and morphology of small spheres, forming a dense agglomerate. Nevertheless, there was no evidence of formation of microporosity.[31] Shen et al. treated chitosan at temperatures ranging from 140 to 220 °C for 10 h. They observed that the produced materials presented chemical stability in acidic solutions and that the amino groups were completely retained in the structure.[32] Some studies report the use of chitosan hydrochars as precursors of porous carbons. For example, Laginhas et al. revealed that the combination of HTC with activation is an excellent way to produce porous carbons with a high nitrogen content.[33]

Recent studies have reported the use of chitosan hydrochars for the removal of pollutants[32,34−36] and the production of materials for energy storage.[37,38] Nevertheless, to the best of our knowledge, there is no reported study on the use of chitosan hydrochars for CO_2 capture. In this work, we report the effects of HTC time on chitosan's chemical properties and its CO_2 capture potential. HTC allows changes in chitosan's surfaces and structural properties, increasing the CO_2 adsorption capacity by 4-fold.

RESULTS AND DISCUSSION

Chemical Composition—CNH Elemental Analysis. Table 1 shows the chemical composition of the parent chitosan and HTC materials. Chitosan presented a carbon content around 39 wt %, whereas this percentage increases in the HTC samples, being above 48 wt % for the HTC material treated for 48 h. On the other hand, the oxygen content goes in the opposite direction, being 46 wt % in the parent chitosan and around 37 wt % in CHIT-HTC-48. Figure S1 presents the atomic ratios of the hydrochars. The atomic O/C and H/C ratios decrease with the increase of HTC time, but some fluctuation occurs at the beginning of the HTC series. These results are consistent with the dehydration of the biomass forming a carbon-rich structure, possibly of more aromatic nature. The relative nitrogen content was virtually the same in all the materials; it is 7.3 wt % in the parent chitosan and accounts for 7.5 wt % in CHIT-HTC-48. The atomic N/C ratio, however, decreases upon HTC. This result indicates that most of the nitrogen atoms remain in the structure of the adsorbent upon HTC, probably conferring basic properties to the materials. The volatile amine compounds, if produced, can further react with the carbonaceous scaffold, as previously reported,[46,47] but we were unable to prove that in the experiments. After 48 h of HTC, the carbon content increases from 39 to 48 wt %, whereas the nitrogen content virtually stays the same. This implies that nitrogen atoms are incorporated within the carbon matrix during HTC, perhaps, probably forming aromatic amines for longer times of heat treatment.[48] The higher heating values (HHVs) of the HTC chitosan materials were between 15 and 19 MJ/kg, as shown in Table 1.

Structural Characterization by FTIR Analysis. Figure S2 shows the FTIR spectra of the chitosan and HTC samples. The spectrum of chitosan shows a broad band at 3372 cm^{-1} related to the hydroxyl groups. The intensity and broadness of this band overlap the two sharp bands located at 3440 and 3372 cm^{-1}, which are related to NH asymmetric and symmetric stretching vibrations, respectively. C−H asymmetric and symmetric stretching at 2930 and 2880 cm^{-1}, respectively, can also be observed. The band at 1650 cm^{-1} can be related to C═O stretching in amides and may be due to the incomplete hydrolysis of the chitin precursor. The band at 1600 cm^{-1} may be related to NH_2 deformation. The C−O−C stretching vibration can be highlighted at 1252 cm^{-1}. The region between 1150 and 1025 cm^{-1} corresponds to the stretching vibrations of C−O, C−N, and C−C. In addition, the band at 895 cm^{-1} is related to C−H and NH_2 deformation and O−H out-of-plane deformation.[49,50]

The spectra of the HTC materials show some remarkable changes relative to chitosan. The most noticeable is the decrease in intensity of the broad OH band at 3372 cm^{-1}, which is consistent with dehydration of the polysaccharide. Hence, the bands at 3440 and 3372 cm^{-1}, related to NH stretching, can be better observed in the HTC materials. It is possible to identify the presence of aliphatic structures characterized by the bands of C−H stretching at 2930 and

https://dx.doi.org/10.1021/acsomega.0c04470
ACS Omega 2020, 5, 29520−29529

2880 cm^{-1}.[26,33] Figure S3 shows an amplification of the region between 1200 and 1600 cm^{-1} to highlight the bands at 1323 cm^{-1}, which can be related to the C−N stretching in aromatic amines; it also amplifies the region between 1150 and 800 cm^{-1} to show the C−O stretching vibration at 1070 cm^{-1}, which may be characteristic of aromatic systems.[38,51]

Structural Characterization by ^{13}C CP-MAS/NMR Analysis. Figure S4 shows the ^{13}C CP-magic-angle spinning (MAS)/NMR spectra of chitosan and the HTC adsorbents. The spectrum of chitosan presents a similar profile of published literature results.[52] The signals at 23 and 175 ppm correspond to residual acetyl groups (4%), relative to the chitin precursor, calculated as indicated in the literature.[39] The signals in the region between 50 and 110 ppm correspond to the C1−C6 carbon atoms of the *N*-acetyl glucosamine unit. For the HTC samples, the attribution can be done as follows: δ = 10−50 ppm corresponds to aliphatic CH_x groups; δ = 110−150 ppm may be related to aromatic rings, mostly of furanic nature. This trend is more evidenced in the samples treated at longer periods (6−48 h), which confirms the more aromatic nature of the HTC materials as the time of HTC increases.

At 180 °C, even for low reaction times (1 h), the hydrolysis of β-1.4 bonds has already occurred, which might be evidenced by the second signal observed at around 105 ppm that is absent in the parent chitosan. Upon increasing the HTC time, a decrease in the signal intensity of the C1 chitosan signal at 105 ppm was observed, together with the appearance of signals in the regions between 120 and 140 ppm and from 20 to 50 ppm, corresponding to sp^2 and sp^3 carbon atoms, respectively. Simsir and collaborators studied the HTC of chitosan for 24 h and observed the formation of sp^2 carbon atoms, in a relatively more intense quantity than that obtained in our experiments.[27] This can be attributed to the chitosan/water mass ratio, and especially to the temperature used, which were higher than the conditions used in this work.

Figure 1a shows the relation between the NMR signal areas and the time of treatment. It can be clearly seen that the signal at 105 ppm, associated with O−C−O groups (glycosidic bond), decreases with the time of treatment, whereas the signal at 125 ppm, associated with aromatic carbon atoms, increases.

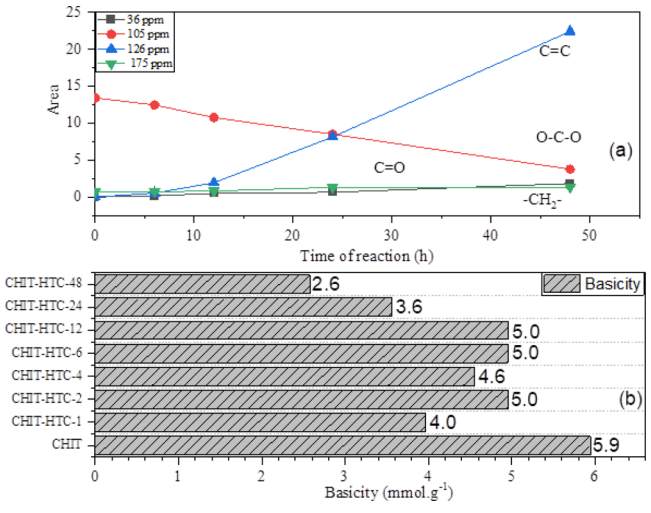

Figure 1. Variation of the signal areas of the ^{13}C CP-MAS-NMR spectra corresponding to O−C−O, CH_2, C═O, and C═C groups (a) and basicity of the parent chitosan and HTC samples, as measured with a diluted HCl solution (b).

The methyl and carbonyl composition are practically constant over time due to the thermal stability of the acetylated units. Therefore, the ^{13}C solid-state CP-MAS/NMR analysis shows that the hydrothermal treatment at longer periods potentializes the carbonization process toward a more aromatic structure, probably with furanic domains.[38,51]

Basicity Measurements. The potentiometric titration curves of the parent chitosan and HTC samples are presented in Figure S5. As the pK_a of chitosan is around 6.5, it is solubilized in aqueous acid solutions (pH 2). Therefore, the chitosan curve presents two inflection points: the first is due to neutralization of the excess of HCl, whereas the second is related to the neutralization of the protonated amine groups of the chitosan structure. Although the HTC materials still preserve the glucosamine units, as seen in the structural characterization, the titration curves for all carbon samples have only one inflection point, indicating that the protonation of the basic sites does not result in the solubilization of the material. This chemical stability in the acid medium is due to the aromatization/pseudographitization of the structure upon hydrothermal treatment.[26,32]

The basicity of the samples was calculated considering the volume of the equivalence point, determined by the first derivative of the potentiometric curves. In general, the basicity of chitosan is higher than the basicity of the HTC materials, especially for the HTC samples treated at 24 and 48 h (Figure 1b), even though the nitrogen content of the materials is virtually the same. These results can be explained by the structural changes resulting from HTC, which indicated a more aromatic structure as the time of HTC increases. Therefore, aromatic amines should be formed during HTC, which are known to be weaker bases than aliphatic amines. As the nitrogen content is virtually the same in all the materials, the difference in basicity may be associated with the formation of weaker basic sites that might not be protonated in diluted HCl solutions.

Figure S6 shows the basicity of the CHIT-HTC-48 materials using more concentrated hydrochloric acid solutions (1.3 and 4.1 $mol{\cdot}L^{-1}$). One can observe that the total basicity increases about 10- to 16-fold compared to that in the diluted HCl concentration (0.1 $mol{\cdot}L^{-1}$). These data reinforce the hypothesis of the formation of weaker basic sites, probably of aromatic nature, upon HTC of chitosan.

Thermal Analysis. The thermal decomposition of chitosan and HTC samples, under nitrogen flow, was monitored by TGA and is presented in Figure S7. Table S1 also shows the weight loss at the corresponding temperature of the maximum loss in each step. Chitosan showed two thermal degradation processes. The first is related to the loss of adsorbed water and represents around 10% of weight loss. It is worth mentioning that this process occurs up to 140 °C because of hydrogen bonding between the polysaccharide and the water molecules.[53] The second thermal degradation occurs around 311 °C and corresponds to 47% weight loss. This step can be attributed to the degradation of chitosan, with dehydration and deacetylation of the structure.[54]

The HTC samples have similar decomposition patterns, presenting two main events of weight loss. As a general trend, the first process of weight loss is similar for all samples and the parent chitosan material, representing about 10%. However, the HTC samples present a smaller weight loss for the second step, around 310 °C, compared with chitosan. The decrease is more prominent for the materials treated for longer times. For

https://dx.doi.org/10.1021/acsomega.0c04470
ACS Omega 2020, 5, 29520−29529

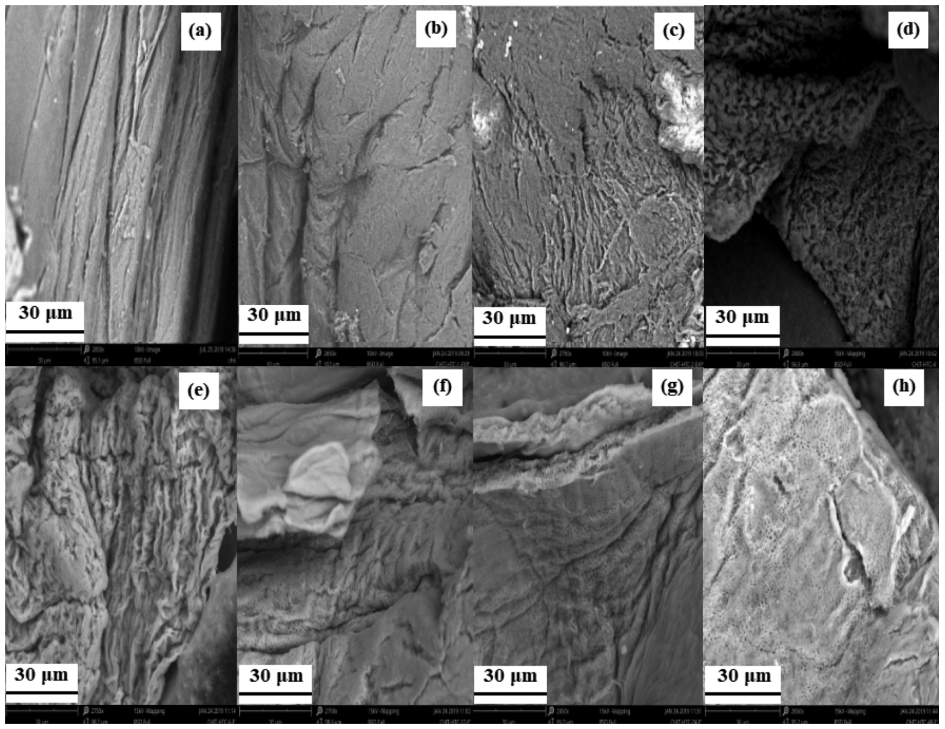

Figure 2. SEM image of materials: (a) chitosan, (b) CHIT-HTC-1, (c) CHIT-HTC-2, (d) CHIT-HTC-4, (e) CHIT-HTC-6, (f) CHIT-HTC-12, (g) CHIT-HTC-24, and (h) CHIT-HTC-48.

Table 2. Composition Ratio, Basicity, and CO_2 Uptake Data of the Parent Chitosan and HTC Materials

	H/C	O/C	N/C	basicity (mmol·g^{-1})	CO_2 uptake (mmol·g^{-1})	$\Delta G°$ (kJ·mol^{-1})
CHIT	0.17	1.15	0.18	5.9	0.10	−6.43
CHIT-HTC-12	0.16	1.06	0.18	5.0	0.10	−2.41
CHIT-HTC-24	0.15	0.97	0.16	3.6	0.30	−3.63
CHIT-HTC-48	0.13	0.77	0.15	2.6	0.45	−3.15

	Langmuir			Freundlich		
	K_L (bar^{-1})	q_m (mmol·g^{-1})	R^2	K_F (mmol$^{1-(1/n)}$·g$^{1/n}$·g^{-1})	n	R^2
CHIT	13.4	0.13	0.994	0.12	3.6	0.880
CHIT-HTC-12	2.6	0.17	0.928	0.13	2.4	0.954
CHIT-HTC-24	4.3	0.40	0.974	0.34	3.1	0.980
CHIT-HTC-48	3.6	0.55	0.978	0.44	2.6	0.995

	pseudo-first order			pseudo-second order		
	q_e (mmol g^{-1})	k_1 (min^{-1})	R^2	q_e (mmol·g^{-1})	k_2 (g·mmol^{-1}·min^{-1})	R^2
CHIT	0.10	0.78	0.992	0.11	15.3	0.999
CHIT-HTC-12	0.16	0.76	0.991	0.14	6.8	0.996
CHIT-HTC-24	0.33	0.76	0.991	0.34	3.7	0.997
CHIT-HTC-48	0.44	0.77	0.992	0.47	3.2	0.999

instance, the samples carbonized at 24 and 48 h showed a weight loss of approximately 38 and 31%, respectively. This fact agrees with the CHN results, which indicated a less oxygenated structure as the time of HTC increases. It may also suggest that these materials have a more aromatic character.

Scanning Electron Microscopy. Figure 2 shows the SEM images of chitosan and HTC samples. It can be observed that chitosan presents a dense morphology with smooth regions, whereas the hydrochars exhibit a more irregular morphology. Materials treated for 1, 2, 4, and 6 h have a rougher surface and do not exhibit porosity. This morphology is the result of the polymer dehydration process that occurs in shorter times of treatment, as shown by structural characterization and chemical composition analyses. On the other hand, the materials treated between 12 and 48 h present clusters and small porous surfaces. This can be attributed to the aromatization process of the polymer structure, which is expected to form interspersed clusters of small spheres that lead to a monolithic structure with interstitial macroporosity.[48]

Textural Properties. Figure S8 shows the nitrogen adsorption isotherms of chitosan and HTC materials. All samples displayed type III adsorption isotherms, characteristic of nonporous or macroporous materials.[55] The shape of the isotherms indicates interparticle adsorption, implying that the structure of the hydrochars shows clusters of small particles, in agreement with the SEM analysis.

Table S2 reports the surface areas of chitosan and hydrochars. One can see that the Brunauer−Emmett−Teller

https://dx.doi.org/10.1021/acsomega.0c04470
ACS Omega 2020, 5, 29520−29529

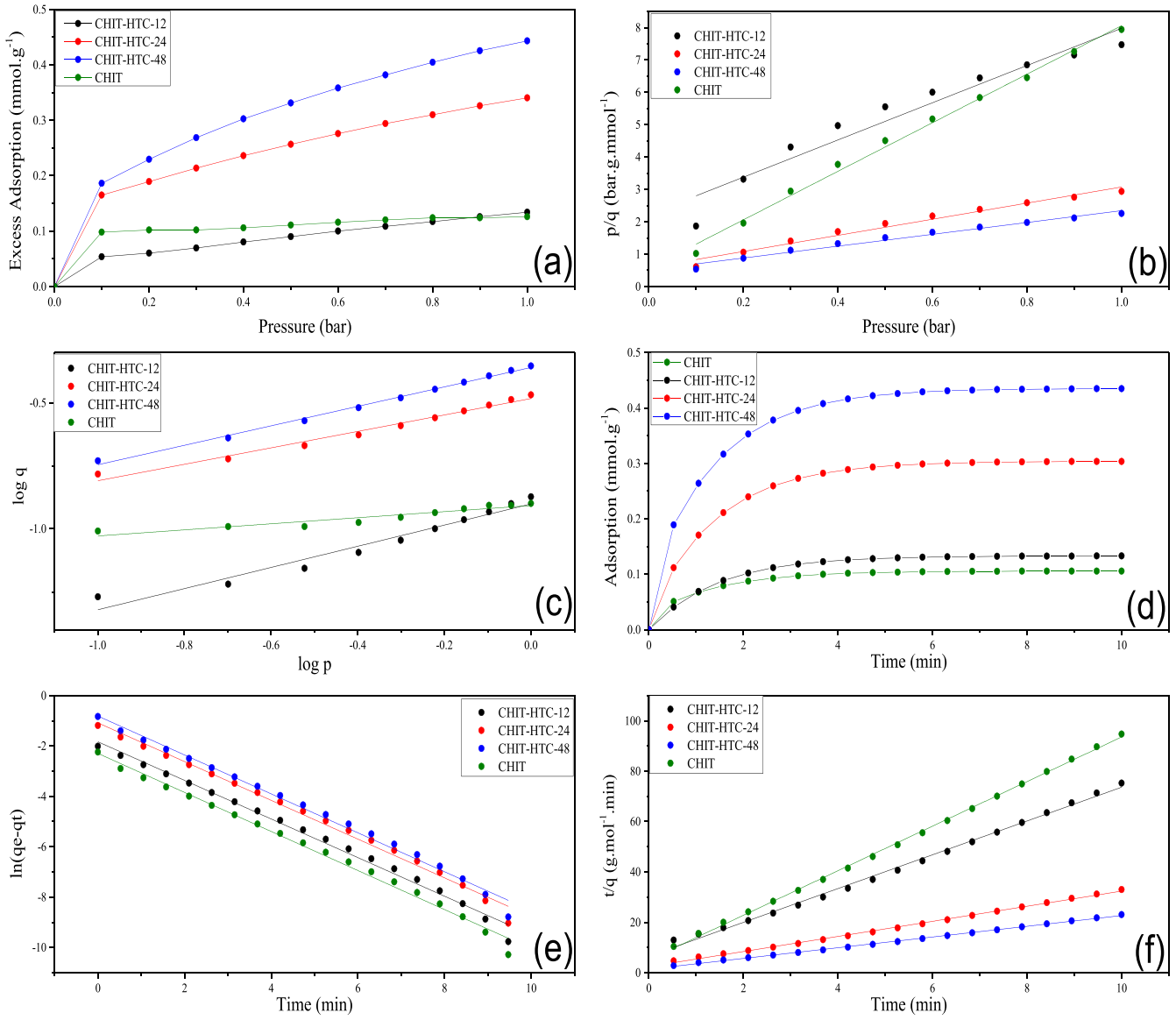

Figure 3. CO_2 adsorption isotherms (a), linearized adsorption models of CO_2 adsorption: Langmuir (b) and Freundlich (c), kinetic curves of CO_2 adsorption (d), kinetic plot of pseudo-first order (e) and pseudo-second order (f) for the adsorption of CO_2 on chitosan and HTC materials.

(BET) specific surface areas are low and no porosity has been identified. Although the HTC samples treated between 12 and 48 h have developed some porosity, as seen from the SEM image, this porosity may be associated with the formation of monoliths from glucosamine units or the reduction of the size of aggregate particles.[56]

CO_2 Adsorption Measurements. As the structural and chemical composition analyses showed similarities between the parent chitosan and the HTC materials treated for shorter time periods, we decided to evaluate the CO_2 uptake of only the HTC materials treated for 12, 24, and 48 h, as well as the parent chitosan for comparison purposes. The CO_2 adsorption capacities are in the range of 0.10−0.45 mmol·g^{-1} depending on the time of treatment (Table 2). As expected, CHIT-HTC-12 showed a CO_2 uptake similar to that of the parent chitosan, around 0.10 mmol·g^{-1}, whereas the HTC materials treated for 24 and 48 h are significantly more efficient for CO_2 capture, presenting uptakes of 0.30 and 0.45 mmol·g^{-1}, respectively. All samples presented type II isotherms (Figure 3a), which are typical of nonporous or macroporous materials, according to the IUPAC classification.[55] The results refer to 25 °C and 1 atm.

Although the nitrogen content and surface area of the HTC materials and of the parent chitosan are similar, the CO_2 uptake of the HTC samples treated at 24 and 48 h is significantly higher, meaning that they are better adsorbents for CO_2 capture. Considering that CO_2 adsorption is mostly due to the acid−base interaction with the adsorbents, one must conclude that not all the nitrogen atoms in the parent chitosan are available for adsorption. Intense intra- and intermolecular hydrogen bonds may occur in the chitosan structure, making the NH_2 moiety less prone to interaction with the CO_2 molecule. In addition, the structure of the polymer may be folded to maximize the interaction within the chain, also contributing to the decrease of the effective nitrogen atoms available for CO_2 adsorption. On the other hand, upon HTC and consequent aromatization of the materials, the structure of the adsorbent may become less folded and the nitrogen atoms more available to interact with the CO_2 molecule, explaining

https://dx.doi.org/10.1021/acsomega.0c04470
ACS Omega 2020, 5, 29520−29529

the higher adsorption capacity of the materials with respect to the parent chitosan.

In order to describe the adsorbent−adsorbate interactions, we fitted the data to the Langmuir (eq 1) and Freundlich (eq 2) isotherms and obtained the linearized graphs of the models (Figure 3b,c). The parameters and the respective correlation coefficients (R^2) for each material are reported in Table 2.

$$\frac{p}{q_e} = \frac{1}{q_m K_L} + \frac{1}{q_m} p \quad (1)$$

$$\ln q_e = \ln K_F + \frac{1}{n} \ln p \quad (2)$$

Here, q_e is the amount of CO_2 adsorbed per mass unit of the adsorbent at equilibrium (mmol·g^{-1}), q_m is the maximum adsorption capacity (mmol·g^{-1}), p is the equilibrium pressure (bar), K_L is the Langmuir constant related to the free energy of adsorption (g·mmol^{-1}), and K_F (mmol$^{1-(1/n)}$·g$^{1/n}$·g^{-1}) and n (dimensionless) are constants of the Freundlich model related to the capacity and intensity of the adsorption process, respectively.

Based on the correlation coefficient (R^2), the experimental data for the parent chitosan fits better with the Langmuir isotherm model. The CHIT-HTC-12 material showed an intermediate behavior, indicating that neither models are completely in agreement with the data fitting. CHIT-HTC-24 and especially the CHIT-HTC-48 adsorbents fitted better with the Freundlich model, indicating that the energy of interaction between these materials and the CO_2 molecule is not constant across the surface of the adsorbents. This may suggest that different types of basic groups, with different basic strength, might be present on the surface of the HTC materials.

The Langmuir isotherm describes adsorption to form a monolayer, in which it is assumed that adsorption occurs on energetically equivalent sites.[42] Nonetheless, adsorption on energetically equivalent surfaces and without interaction between the adsorbate molecules is rare in practice.[57] In this context, the Freundlich isotherm is better applied to describe the adsorption on nonuniform surfaces and takes into account the interaction between the adsorbed molecules.

The better fitting of the parent chitosan to the Langmuir model is in agreement with the nature of the basic sites, all of the same general structure, which implies that the energy of adsorption should be similar, as predicted by the model. On the other hand, the adsorption of CO_2 on the HTC materials treated for longer times showed better fitting with the Freundlich model, indicating different processes of adsorption on the surfaces, probably arising from different structural adsorption sites. The parameter n indicates the heterogeneity of the adsorption sites. The greater the value is, the larger is the difference in the energy of adsorption between the sites of the material. The adsorption process is favorable when n is between 1 and 10.[58]

The change in Gibbs-free energy (eq 3) can be determined using the K_L, previously calculated from the adjustment of the experimental data for the Langmuir model.

$$\Delta G^\circ = -RT \ln K_L \quad (3)$$

where R is the universal ideal gas constant (8.314 J·mol^{-1}·K^{-1}) and T is the absolute temperature (K).

Table 2 shows the Gibbs-free energy change (ΔG°), calculated with the data from the Langmuir constant (K_L).[57] The ΔG° is negative for all adsorbents, indicating that the CO_2 adsorption process on the surface of chitosan and HTC materials is favorable and spontaneous at 25 °C. Furthermore, chitosan is the material that has the most negative ΔG° value, suggesting that the interaction of the CO_2 molecule with the basic sites of the chitosan material is stronger when compared to the interaction on the HTC materials. It must be stressed, however, that these results should be analyzed with care, as the Langmuir model was not the best to describe the adsorption on the HTC materials.

Figure 3d shows the kinetic plot of CO_2 adsorption for chitosan and the HTC materials at 25 °C and 1 bar. The adsorption is fast and equilibrium is reached at short contact times. This is probably because of the fast acid−base reaction between the CO_2 molecule and the nitrogen basic groups of the adsorbents. Hence, the external surface is saturated and may hinder the diffusion process.[59] In terms of CO_2 adsorption capacity, chitosan and HTC-12 showed similar values, around 0.10 mmol·g^{-1}. The materials hydrothermally carbonized at longer times presented higher adsorption capacity. The value of CHIT-HTC-24 was 0.30 mmol·g^{-1}, whereas CHIT-HTC-48 adsorbs 0.45 mmol·g^{-1} of CO_2.

In the pseudo-first-order kinetic model, the adsorption rate is proportional to the number of free adsorption sites on the adsorbent.[60−64] Equation 4 presents the linear relationship of this model

$$\ln(q_e - q_t) = \ln q_e - k_1 t \quad (4)$$

The term q_t (mmol·g^{-1}) is the quantity of gas adsorbed at a given time; q_e (mmol·g^{-1}) is the adsorption capacity at equilibrium; and k_1 (min^{-1}) is the first-order kinetic constant.

In the pseudo-second-order kinetic model, it is assumed that the gas adsorption rate is related to the square of the number of unoccupied sites.[60−64] Equation 5 presents a linear relationship with the model

$$\frac{t}{q_t} = \frac{1}{k_2 q_e^2} + \frac{1}{q_e} t \quad (5)$$

Here, k_2 (g·mmol^{-1}·min^{-1}) is the second-order kinetic constant.

Figure 3e,f shows the plots, whereas Table 2 presents the kinetic constant and the correlation coefficient. It can be observed that the pseudo-second-order kinetic model shows a slightly better fit than the pseudo-first-order kinetic model. This is probably because the pseudo-first-order kinetic model describes, more appropriately, the physisorption of gases on adsorbents, pointing out the reversibility of the equilibrium established between the gas−solid interactions. On the other hand, the kinetic model of pseudo-second order usually describes the chemisorption of a gas on an adsorbent, assuming that the kinetics of adsorption is controlled by the reaction between the adsorbate and the adsorbent.[59,60,64−68] Thus, the results suggest that the kinetics of adsorption is controlled by the acid−base reaction between the CO_2 molecule and the basic sites of the materials, associated with the presence of nitrogen atoms.

The adsorption values at equilibrium, determined by the two kinetic models, show good agreement with the experimental values. The kinetic constant k_1 is almost the same for all materials, around 0.8 min^{-1}, whereas k_2 changes significantly with the time of HTC. Chitosan presented the highest k_2 value, around 15 g·mmol^{-1}·min, but the values decrease for the HTC materials as a function of time of treatment. The results

https://dx.doi.org/10.1021/acsomega.0c04470
ACS Omega 2020, 5, 29520−29529

indicate that equilibrium is reached faster on the parent chitosan than on the HTC materials. A possible explanation is related to the nature of basic sites on the materials and the respective strength. On the parent chitosan, the basic sites are of similar nature and strength, as suggested by the better fitting to the Langmuir isotherm. On the other hand, the HTC materials treated for longer times present a more heterogeneous structure, possibly of aromatic nature, indicative of different basic strengths. Therefore, the kinetics of adsorption may be slower compared with that of the parent chitosan.

CONCLUSIONS

The HTC of chitosan afforded materials with increased carbon content. The relative amount of carbon atoms increases with the time of HTC treatment, whereas the oxygen content goes in the opposite direction. The amount of nitrogen atoms in the HTC samples did not significantly change relative to the parent chitosan. Structural characterization of the HTC materials revealed a more aromatic structure for longer reaction times. Nevertheless, SEM analyses, as well as textural characterization, revealed that the materials did not develop significant porosity. The basicity of the HTC adsorbents decreased relative to the parent chitosan, in spite of the same nitrogen content, which may be interpreted in terms of the strength of the basic sites. Upon HTC, aromatic amines could be formed, which are known to be weaker bases. The HTC materials treated for longer times showed a higher CO_2 adsorption capacity but a reduced basicity than that of the parent chitosan and almost the same nitrogen atom content as the parent chitosan. This implies that part of the nitrogen atoms in the chitosan are not available for CO_2 adsorption, whereas HTC leads to a more aromatic structure, probably exposing the nitrogen atoms. The adsorption data of the HTC samples were better fitted by the Freundlich isotherm and the pseudo-second-order kinetic model, implying the presence of different types of basic groups on the adsorbent. This is consistent with the process of aromatization of the structure, yielding different types of basic aromatic amine groups.

EXPERIMENTAL SECTION

Materials. Chitosan was purchased from Polymar (Brazil), lot number 01012017, and showed a deacetylation degree of 96%, as determined by CP-MAS ^{13}C NMR, according to the literature procedure.[39] The intrinsic viscosity η = 0.325 $L{\cdot}g^{-1}$ and the average viscosimetric molar mass $M_v = 1.7 \times 10^5$ $g{\cdot}mol^{-1}$, as determined by the Mark−Hounwink−Sakurada equation (eq 6).

$$[\eta] = K \times M_v^a \tag{6}$$

Here, K is 0.00181 $mL{\cdot}g^{-1}$ and a is 0.93 for a chitosan solution using 0.1 $mol{\cdot}L^{-1}$ acetic acid and 0.2 $mol{\cdot}L^{-1}$ sodium chloride buffer at 25 °C.

HTC of Chitosan. The HTC materials were synthesized by hydrothermal treatment of chitosan according to the following procedure: typically, 4 g of chitosan (CHIT) was suspended in 40 mL of deionized water to achieve a mass/volume ratio of 1CHIT/10H_2O. Then, the suspension was transferred to a stainless-steel autoclave and heated to 180 °C under autogenous pressure for different times (1, 2, 4, 6, 12, 24, and 48 h). At the end, the autoclave was immediately cooled in cold water, the mixture was filtered, and the solid product was collected and washed several times with distilled water until pH ∼ 7. The resulting solid materials were dried at 120 °C for 2 h and named CHIT-HTC-*X*, where *X* denotes the reaction time. Upon HTC, the material changes from a pale-yellow color, characteristic of the chitosan material, to dark black, especially for materials treated for longer times.

Chemical and Structural Characterization. The elemental analyses of chitosan and HTC samples were conducted on a PerkinElmer 2400 series II elemental analyzer. The HHVs of the HTC of chitosan were calculated according to Dulong's formula[27] (eq 7).

$$\mathrm{HHV} = (0.338 \times C) + 1.428 \times \left(H - \frac{O}{8}\right) + (0.095 \times S) \tag{7}$$

The chemical structure of the materials was evaluated by FTIR and CP-MAS ^{13}C solid-state NMR spectroscopy. The FTIR spectra were recorded in the range of 400−4000 cm^{-1} with a resolution of 2 cm^{-1} on a Shimadzu IRAffinity-1 equipment. Customarily, 16 scans were signal-averaged to minimize the spectral noise. The ^{13}C solid-state NMR analyses of the samples were performed on a Bruker AVANCE III 400 (9.4 T, with a ^{13}C Larmor frequency of 100.65 MHz) using a triple channel probe with 4.0 mm rotors at a spinning rate of 10 kHz. The ^{13}C NMR spectra were recorded using MAS and cross-polarization (CP ramp) with 3 ms of CP contact time, 3 s of recycle delay, and 4000 transients for each spectrum. The chemical shifts were measured relative to tetramethylsilane. Moreover, the basic functional groups on the surface of the chitosan and HTC materials were evaluated according to the Boehm titration method.[40,41] The thermal structural stability of the hydrochars was evaluated by thermogravimetric analysis performed on a TGA-51 Shimadzu thermogravimetric equipment. For each sample, 5 mg was heated from room temperature to 900 °C at a heating rate of 10 $°C{\cdot}min^{-1}$, under a N_2 atmosphere with a flow rate of 50 $mL{\cdot}min^{-1}$.

Surface Characterization. The morphology of the materials was examined using a scanning electron microscope (Phenon Pro X), operated at an electron-accelerating voltage of 10 kV. Prior to scanning, the samples were kept onto a carbon adhesive tape on an aluminum stub under high vacuum conditions. The surface area and porosity of the chitosan-adsorbent samples were analyzed by nitrogen sorption isotherms, obtained at −196 °C, on the Micromeritics ASAP 2020 equipment. The surface area was determined using the BET method applied to the adsorption data with the relative pressure (P/P_o) ranging from 0.06 to 0.3. The materials were outgassed at 120 °C for 24 h prior to the analyses.

CO_2 Adsorption Experiment. The CO_2 adsorption isotherms of all carbon adsorbents were obtained on a XEMIS 001 gas sorption analyzer from Hiden Isochem. The adsorption process was carried out at 25 °C and at pressures varying from ∼0 to 1000 mbar (100 $mbar{\cdot}min^{-1}$) using pure CO_2. Before the adsorption analysis, each sample was pretreated for 4 h under vacuum at 150 °C. The experimental data were adjusted to the linearized forms of the Langmuir and Freundlich adsorption isotherms.[42,43] Kinetic models, such as pseudo-first order[44] and pseudo-second order,[45] were used to develop the kinetic study of CO_2 adsorption on the HTC chitosan materials. The linear correlation coefficient (R^2) was used as a selection criterion for the best-fitted model describing the adsorption process.

https://dx.doi.org/10.1021/acsomega.0c04470
ACS Omega 2020, 5, 29520−29529

■ ASSOCIATED CONTENT

Supporting Information

The Supporting Information is available free of charge at https://pubs.acs.org/doi/10.1021/acsomega.0c04470.

H/C, O/C, and N/C atomic ratios of HTC chitosan materials as a function of treatment time; FTIR spectra of chitosan and HTC samples HTC-1, HTC-2, HTC-4, HTC-6HTC-12, HTC-24, and HTC-48; amplification of the 1600−1200 and 1150−800 cm^{-1} regions of the FTIR spectra of chitosan and HTC samples; ^{13}C CP-MAS/NMR spectra of chitosan, CHIT-HTC-1, CHIT-HTC-2, CHIT-HTC-4, CHIT-HTC-6, CHIT-HTC-12, CHIT-HTC-24, and CHIT-HTC-48; potentiometric titration curves of chitosan and HTC samples; basicity of the CHIT-HTC-48 material at different HCl concentrations; DTG curves of chitosan, CHIT-HTC-1, CHIT-HTC-2, CHIT-HTC-4, CHIT-HTC-6, CHIT-HTC-12, CHIT-HTC-24, and CHIT-HTC-48; weight loss and temperature corresponding to the maximum loss in each step for chitosan and HTC samples; nitrogen adsorption isotherms of chitosan and HTC materials; and textural properties of the HTC samples (PDF)

■ AUTHOR INFORMATION

Corresponding Author

Claudio J. A. Mota − *Instituto de Química and Escola de Química, Universidade Federal do Rio de Janeiro, Rio de Janeiro, RJ 21941-909, Brazil; INCT Energia & Ambiente, UFRJ, Rio de Janeiro, RJ 21941-909, Brazil;* orcid.org/0000-0002-8130-1192; Email: cmota@iq.ufrj.br

Authors

José A. O. Chagas − *Instituto de Química, Universidade Federal do Rio de Janeiro, Rio de Janeiro, RJ 21941-909, Brazil;* orcid.org/0000-0001-5252-2992

Gustavo O. Crispim − *Escola de Química, Universidade Federal do Rio de Janeiro, Rio de Janeiro, RJ 21941-909, Brazil*

Bianca P. Pinto − *Instituto de Química, Universidade Federal do Rio de Janeiro, Rio de Janeiro, RJ 21941-909, Brazil; INCT Energia & Ambiente, UFRJ, Rio de Janeiro, RJ 21941-909, Brazil;* orcid.org/0000-0002-0645-5896

Rosane A. S. San Gil − *Instituto de Química and Instituto de Pesquisas de Produtos Naturais, Universidade Federal do Rio de Janeiro, Rio de Janeiro, RJ 21941-909, Brazil*

Complete contact information is available at: https://pubs.acs.org/10.1021/acsomega.0c04470

Notes

The authors declare no competing financial interest.

■ ACKNOWLEDGMENTS

The authors acknowledge financial support from Shell Brazil, CNPq, CAPES, and FAPERJ. The NQTR (IQ-UFRJ) is acknowledged for SEM analysis.

■ REFERENCES

(1) Kriegler, E.; Bauer, N.; Popp, A.; Humpenöder, F.; Leimbach, M.; Strefler, J.; Baumstark, L.; Bodirsky, B. L.; Hilaire, J.; Klein, D.; Mouratiadou, I.; Weindl, I.; Bertram, C.; Dietrich, J.-P.; Luderer, G.; Pehl, M.; Pietzcker, R.; Piontek, F.; Lotze-Campen, H.; Biewald, A.; Bonsch, M.; Giannousakis, A.; Kreidenweis, U.; Müller, C.; Rolinski, S.; Schultes, A.; Schwanitz, J.; Stevanovic, M.; Calvin, K.; Emmerling, J.; Fujimori, S.; Edenhofer, O. Fossil-Fueled Development (SSP5): An Energy and Resource Intensive Scenario for the 21st Century. *Global Environ. Change* **2017**, *42*, 297−315.

(2) Lakhi, K. S.; Park, D.-H.; Singh, G.; Talapaneni, S. N.; Ravon, U.; Al-Bahily, K.; Vinu, A. Energy Efficient Synthesis of Highly Ordered Mesoporous Carbon Nitrides with Uniform Rods and Their Superior CO_2 Adsorption Capacity. *J. Mater. Chem. A* **2017**, *5*, 16220−16230.

(3) Fasihi, M.; Efimova, O.; Breyer, C. Techno-Economic Assessment of CO_2 Direct Air Capture Plants. *J. Cleaner Prod.* **2019**, *224*, 957−980.

(4) Schleussner, C.-F.; Rogelj, J.; Schaeffer, M.; Lissner, T.; Licker, R.; Fischer, E. M.; Knutti, R.; Levermann, A.; Frieler, K.; Hare, W. Science and Policy Characteristics of the Paris Agreement Temperature Goal. *Nat. Clim. Change* **2016**, *6*, 827−835.

(5) Rao, A. B.; Rubin, E. S. A Technical, Economic, and Environmental Assessment of Amine-Based CO_2 Capture Technology for Power Plant Greenhouse Gas Control. *Environ. Sci. Technol.* **2002**, *36*, 4467−4475.

(6) Figueroa, J. D.; Fout, T.; Plasynski, S.; Mcilvried, H.; Srivastava, R. D. Advances in CO_2 Capture Technology — The U . S . Department of Energy' s Carbon Sequestration Program. *Greenh. Gas Contr.* **2008**, *2*, 9−20.

(7) Dutcher, B.; Fan, M.; Russell, A. G. Amine-Based CO_2 Capture Technology Development from the Beginning of 2013 - A Review. *ACS Appl. Mater. Interfaces* **2015**, *7*, 2137−2148.

(8) Chen, T.; Deng, S.; Wang, B.; Huang, J.; Wang, Y.; Yu, G. CO_2 Adsorption on Crab Shell Derived Activated Carbons: Contribution of Micropores and Nitrogen-Containing Groups. *RSC Adv.* **2015**, *5*, 48323−48330.

(9) Didas, S. A.; Choi, S.; Chaikittisilp, W.; Jones, C. W. Amine-Oxide Hybrid Materials for CO_2 Capture from Ambient Air. *Acc. Chem. Res.* **2015**, *48*, 2680−2687.

(10) Liu, L.; Jin, S.; Ko, K.; Kim, H.; Ahn, I.-S.; Lee, C.-H. Alkyl-Functionalization of (3-Aminopropyl)Triethoxysilane-Grafted Zeolite Beta for Carbon Dioxide Capture in Temperature Swing Adsorption. *Chem. Eng. J.* **2020**, *382*, 122834.

(11) Licciulli, A.; Notaro, M.; De Santis, S.; Terreni, C.; Kunjalukkal Padmanabhan, S. CO_2 Capture on Amine Impregnated Mesoporous Alumina-Silica Mixed Oxide Spheres. *Fuel Process. Technol.* **2017**, *166*, 202−208.

(12) Irani, M.; Jacobson, A. T.; Gasem, K. A. M.; Fan, M. Facilely Synthesized Porous Polymer as Support of Poly(Ethyleneimine) for Effective CO_2 Capture. *Energy* **2018**, *157*, 1−9.

(13) Hu, X.; Liu, L.; Luo, X.; Xiao, G.; Shiko, E.; Zhang, R.; Fan, X.; Zhou, Y.; Liu, Y.; Zeng, Z.; Li, C. e. A Review of N-Functionalized Solid Adsorbents for Post-Combustion CO_2 Capture. *Appl. Energy* **2020**, *260*, 114244.

(14) Fan, X.; Zhang, L.; Zhang, G.; Shu, Z.; Shi, J. Chitosan Derived Nitrogen-Doped Microporous Carbons for High Performance CO_2 Capture. *Carbon* **2013**, *61*, 423−430.

(15) Calvo-Muñoz, E. M.; García-Mateos, F. J.; Rosas, J. M.; Rodríguez-Mirasol, J.; Cordero, T. Biomass Waste Carbon Materials as Adsorbents for CO_2 Capture under Post-Combustion Conditions. *Front. Mater.* **2016**, *3*, 1−14.

(16) Rashidi, N. A.; Yusup, S. An Overview of Activated Carbons Utilization for the Post-Combustion Carbon Dioxide Capture. *J. CO_2 Util.* **2016**, *13*, 1−16.

(17) Li, D.; Zhou, J.; Zhang, Z.; Li, L.; Tian, Y.; Lu, Y.; Qiao, Y.; Li, J.; Wen, L. Improving Low-Pressure CO_2 Capture Performance of N-Doped Active Carbons by Adjusting Flow Rate of Protective Gas during Alkali Activation. *Carbon* **2017**, *114*, 496−503.

(18) Wu, Q.; Zhang, G.; Gao, M.; Huang, L.; Li, L.; Liu, S.; Xie, C.; Zhang, Y.; Yu, S. N-Doped Porous Carbon from Different Nitrogen Sources for High-Performance Supercapacitors and CO_2 Adsorption. *J. Alloys Compd.* **2019**, *786*, 826−838.

(19) Rinaudo, M.; Ã, M. R. Chitin and Chitosan: Properties and Applications. *Prog. Polym. Sci.* **2006**, *31*, 603−632.

(20) Sneddon, G.; Ganin, A. Y.; Yiu, H. H. P. Sustainable CO_2 Adsorbents Prepared by Coating Chitosan onto Mesoporous Silicas for Large-Scale Carbon Capture Technology. *Energy Technol.* **2015**, *3*, 249−258.
(21) Danon, A.; Stair, P. C.; Weitz, E. FTIR Study of CO2 Adsorption on Amine-Grafted SBA-15: Elucidation of Adsorbed Species. *J. Phys. Chem. C* **2011**, *115*, 11540−11549.
(22) Pinto, M. L.; Mafra, L.; Guil, J. M.; Pires, J.; Rocha, J. Adsorption and Activation of CO_2 by Amine-Modified Nanoporous Materials Studied by Solid-State NMR and $^{13}CO_2$ Adsorption. *Chem. Mater.* **2011**, *23*, 1387−1395.
(23) Rafigh, S. M.; Heydarinasab, A. Mesoporous Chitosan-SiO_2 Nanoparticles: Synthesis , Characterization and CO_2 Adsorption Capacity. *ACS Sustainable Chem. Eng.* **2017**, *5*, 10379−10386.
(24) Lourenço, M. A. O.; Nunes, C.; Gomes, J. R. B.; Pires, J.; Pinto, M. L.; Ferreira, P. Pyrolyzed Chitosan-Based Materials for CO_2/CH_4 Separation. *Chem. Eng. J.* **2019**, *362*, 364−374.
(25) Huang, C.-C.; Shen, S.-C. Adsorption of CO_2 on Chitosan Modified CMK-3 at Ambient Temperature. *J. Taiwan Inst. Chem. Eng.* **2013**, *44*, 89−94.
(26) Sevilla, M.; Fuertes, A. B. The Production of Carbon Materials by Hydrothermal Carbonization of Cellulose. *Carbon* **2009**, *47*, 2281−2289.
(27) Simsir, H.; Eltugral, N.; Karagoz, S. Hydrothermal Carbonization for the Preparation of Hydrochars from Glucose, Cellulose, Chitin, Chitosan and Wood Chips via Low-Temperature and Their Characterization. *Bioresour. Technol.* **2017**, *246*, 82−87.
(28) Hu, B.; Wang, K.; Wu, L.; Yu, S.-H.; Antonietti, M.; Titirici, M.-M. Engineering Carbon Materials from the Hydrothermal Carbonization Process of Biomass. *Adv. Mater.* **2010**, *22*, 813−828.
(29) Titirici, M.-M.; Antonietti, M. Chemistry and Materials Options of Sustainable Carbon Materials Made by Hydrothermal Carbonization. *Chem. Soc. Rev.* **2010**, *39*, 103−116.
(30) Shen, Y. Review on Hydrothermal Carbonization of Biomass and Plastic Wastes to Energy Products. *Biomass Bioenergy* **2020**, *134*, 105479.
(31) Texter, J.; Zhao, L.; Xiao, P.-W.; Caballero, F. P.; Han, B.-H.; Titirici, M.-M. Connecting Carbon Porosity with Dispersibility and Friability. *Carbon* **2017**, *112*, 117−129.
(32) Shen, F.; Su, J.; Zhang, X.; Zhang, K.; Qi, X. Chitosan-Derived Carbonaceous Material for Highly Efficient Adsorption of Chromium (VI) from Aqueous Solution. *Int. J. Biol. Macromol.* **2016**, *91*, 443−449.
(33) Laginhas, C.; Nabais, J. M. V.; Titirici, M. M. Activated Carbons with High Nitrogen Content by a Combination of Hydrothermal Carbonization with Activation. *Microporous Mesoporous Mater.* **2016**, *226*, 125−132.
(34) Zhou, Q.; Gao, Q.; Luo, W.; Yan, C.; Ji, Z.; Duan, P. One-Step Synthesis of Amino-Functionalized Attapulgite Clay Nanoparticles Adsorbent by Hydrothermal Carbonization of Chitosan for Removal of Methylene Blue from Wastewater. *Colloids Surf., A* **2015**, *470*, 248−257.
(35) Zhao, X.; Ma, X.; Zheng, P. The Preparation of Carboxylic-Functional Carbon-Based Nanofibers for the Removal of Cationic Pollutants. *Chemosphere* **2018**, *202*, 298−305.
(36) He, C.; Lin, H.; Dai, L.; Qiu, R.; Tang, Y.; Wang, Y.; Duan, P.-G.; Ok, Y. S. Waste Shrimp Shell-Derived Hydrochar as an Emergent Material for Methyl Orange Removal in Aqueous Solutions. *Environ. Int.* **2020**, *134*, 105340.
(37) Huang, J.; Liang, Y.; Hu, H.; Liu, S.; Cai, Y.; Dong, H.; Zheng, M.; Xiao, Y.; Liu, Y. Ultrahigh-Surface-Area Hierarchical Porous Carbon from Chitosan: Acetic Acid Mediated Efficient Synthesis and Its Application in Superior Supercapacitors. *J. Mater. Chem. A* **2017**, *5*, 24775−24781.
(38) Aydin, M.; Demir, E.; Unal, B.; Dursun, B.; Ahsen, A. S.; Demir-Cakan, R. Chitosan Derived N-Doped Carbon Coated SnO_2 Nanocomposite Anodes for Na-Ion Batteries. *Solid State Ionics* **2019**, *341*, 115035.
(39) Kasaai, M. R. Determination of the Degree of N-Acetylation for Chitin and Chitosan by Various NMR Spectroscopy Techniques: A Review. *Carbohydr. Polym.* **2010**, *79*, 801−810.
(40) Goertzen, S. L.; Thériault, K. D.; Oickle, A. M.; Tarasuk, A. C.; Andreas, H. A. Standardization of the Boehm Titration. Part I. CO_2 Expulsion and Endpoint Determination. *Carbon* **2010**, *48*, 1252−1261.
(41) Oickle, A. M.; Goertzen, S. L.; Hopper, K. R.; Abdalla, Y. O.; Andreas, H. A. Standardization of the Boehm Titration: Part II. Method of Agitation, Effect of Filtering and Dilute Titrant. *Carbon* **2010**, *48*, 3313−3322.
(42) Langmuir, I. The Constitution and Fundamental Properties of Solids and Liquids. Part I. Solids. *J. Am. Chem. Soc.* **1916**, *38*, 2221−2295.
(43) Redlich, O.; Peterson, D. L. A useful adsorption isotherm. *J. Phys. Chem.* **1959**, *63*, 1024.
(44) Ho, Y. S.; McKay, G. Sorption of Dye from Aqueous Solution by Peat. *Chem. Eng. J.* **1998**, *70*, 115−124.
(45) Blanchard, G.; Maunaye, M.; Martin, G. Removal of Heavy Metals from Waters by Means of Natural Zeolites. *Water Res.* **1984**, *18*, 1501−1507.
(46) Chen, J.; Wang, M.; Ho, C.-T. Volatile Compounds Generated from Thermal Degradation of N -Acetylglucosamine. *J. Agric. Food Chem.* **1998**, *46*, 3207−3209.
(47) Jun, M.; Shao, Y.; Ho, C.-T.; Koetter, U.; Lech, S. Structural Identification of Nonvolatile Dimerization Products of Glucosamine by Gas Chromatography − Mass Spectrometry , Liquid Chromatography − Mass Spectrometry , and Nuclear Magnetic Resonance Analysis. *J. Agric. Food Chem.* **2003**, *51*, 6340−6346.
(48) Zhao, L.; Baccile, N.; Gross, S.; Zhang, Y.; Wei, W.; Sun, Y.; Antonietti, M.; Titirici, M.-M. Sustainable Nitrogen-Doped Carbonaceous Materials from Biomass Derivatives. *Carbon* **2010**, *48*, 3778−3787.
(49) Paluszkiewicz, C.; Stodolak, E.; Hasik, M.; Blazewicz, M. FT-IR Study of Montmorillonite-Chitosan Nanocomposite Materials. *Spectrochim. Acta, Part A* **2011**, *79*, 784−788.
(50) Menezes, J. E. S. A.; Santos, H. S. d.; Ferreira, M. K. A.; Magalhães, F. E. A.; da Silva, D. S.; Bandeira, P. N.; Saraiva, G. D.; Pessoa, O. D. L.; Ricardo, N. M. P. S.; Cruz, B. G.; Teixeira, A. M. R. Preparation, Structural and Spectroscopic Characterization of Chitosan Membranes Containing Allantoin. *J. Mol. Struct.* **2020**, *1199*, 126968.
(51) Gupta, P. K.; Pachauri, N.; Khan, Z. H.; Solanki, P. R. One Pot Synthesized Zirconia Nanoparticles Embedded in Amino Functionalized Amorphous Carbon for Electrochemical Immunosensor. *J. Electroanal. Chem.* **2017**, *807*, 59−69.
(52) Heux, L.; Brugnerotto, J.; Desbrières, J.; Versali, M.-F.; Rinaudo, M. Solid State NMR for Determination of Degree of Acetylation of Chitin and Chitosan. *Biomacromolecules* **2000**, *1*, 746−751.
(53) Zawadzki, J.; Kaczmarek, H. Thermal Treatment of Chitosan in Various Conditions. *Carbohydr. Polym.* **2010**, *80*, 394−400.
(54) Nam, Y. S.; Park, W. H.; Ihm, D.; Hudson, S. M. Effect of the Degree of Deacetylation on the Thermal Decomposition of Chitin and Chitosan Nanofibers. *Carbohydr. Polym.* **2010**, *80*, 291−295.
(55) Thommes, M.; Kaneko, K.; Neimark, A. V.; Olivier, J. P.; Rodriguez-Reinoso, F.; Rouquerol, J.; Sing, K. S. W. Physisorption of Gases, with Special Reference to the Evaluation of Surface Area and Pore Size Distribution (IUPAC Technical Report). *Pure Appl. Chem.* **2015**, *87*, 1051−1069.
(56) Baccile, N.; Antonietti, M.; Titirici, M.-M. One-Step Hydrothermal Synthesis of Nitrogen-Doped Nanocarbons: Albumine Directing the Carbonization of Glucose. *ChemSusChem* **2010**, *3*, 246−253.
(57) Raganati, F.; Alfe, M.; Gargiulo, V.; Chirone, R.; Ammendola, P. Isotherms and Thermodynamics of CO_2 Adsorption on a Novel Carbon-Magnetite Composite Sorbent. *Chem. Eng. Res. Des.* **2018**, *134*, 540−552.

https://dx.doi.org/10.1021/acsomega.0c04470
ACS Omega 2020, 5, 29520−29529

(58) Dada, A. O.; Olalekan, A. P.; olatunya, A. M.; Dada, O. Langmuir, Freundlich, Temkin and Dubinin−Radushkevich Isotherms Studies of Equilibrium Sorption of Zn^{2+} Unto Phosphoric Acid Modified Rice Husk. *IOSR J. Appl. Chem.* **2012**, *3*, 38−45.
(59) Tiwari, D.; Bhunia, H.; Bajpai, P. K. Adsorption of CO_2 on KOH Activated, N-Enriched Carbon Derived from Urea Formaldehyde Resin: Kinetics, Isotherm and Thermodynamic Studies. *Appl. Surf. Sci.* **2018**, *439*, 760−771.
(60) Álvarez-Gutiérrez, N.; Gil, M. V.; Rubiera, F.; Pevida, C. Kinetics of CO_2 Adsorption on Cherry Stone-Based Carbons in CO_2/CH_4 Separations. *Chem. Eng. J.* **2017**, *307*, 249−257.
(61) Song, G.; Zhu, X.; Chen, R.; Liao, Q.; Ding, Y.-D.; Chen, L. An Investigation of CO_2 Adsorption Kinetics on Porous Magnesium Oxide. *Chem. Eng. J.* **2016**, *283*, 175−183.
(62) Balsamo, M.; Tsyntsarski, B.; Erto, A. Dynamic Studies on Carbon Dioxide Capture Using Lignocellulosic Based Activated Carbons. *Adsorption* **2015**, *21*, 633−643.
(63) Singh, J.; Bhunia, H.; Basu, S. CO_2 adsorption on oxygen enriched porous carbon monoliths: Kinetics, isotherm and thermodynamic studies. *J. Ind. Eng. Chem.* **2018**, *60*, 321−332.
(64) Goel, C.; Kaur, H.; Bhunia, H.; Bajpai, P. K. Carbon Dioxide Adsorption on Nitrogen Enriched Carbon Adsorbents: Experimental, Kinetics, Isothermal and Thermodynamic Studies. *J. CO_2 Util.* **2016**, *16*, 50−63.
(65) Keramati, M.; Ghoreyshi, A. A. Improving CO_2 Adsorption onto Activated Carbon through Functionalization by Chitosan and Triethylenetetramine. *Phys. E* **2014**, *57*, 161−168.
(66) Ammendola, P.; Raganati, F.; Chirone, R. CO_2 Adsorption on a Fine Activated Carbon in a Sound Assisted Fluidized Bed: Thermodynamics and Kinetics. *Chem. Eng. J.* **2017**, *322*, 302−313.
(67) Loganathan, S.; Tikmani, M.; Mishra, A.; Ghoshal, A. K. Amine Tethered Pore-Expanded MCM-41 for CO_2 Capture: Experimental , Isotherm and Kinetic Modeling Studies. *Chem. Eng. J.* **2016**, *303*, 89−99.
(68) Loganathan, S.; Tikmani, M.; Edubilli, S.; Mishra, A.; Ghoshal, A. K. CO_2 Adsorption Kinetics on Mesoporous Silica under Wide Range of Pressure and Temperature. *Chem. Eng. J.* **2014**, *256*, 1−8.

https://dx.doi.org/10.1021/acsomega.0c04470
ACS Omega 2020, 5, 29520−29529